Applied Catalysis B: Environmental 307 (2022) 121149

Contents lists available at ScienceDirect

Applied Catalysis B: Environmental

journal homepage: www.elsevier.com/locate/apcatb

Synthesis and bader analyzed cobalt-phthalocyanine modified solar UV-blind β-Ga_2O_3 quadrilateral nanorods photocatalysts for wide-visible-light driven H_2 evolution

Sharafat Ali [a,1], Sajjad Ali [b,1], Pir Muhammad Ismail [a,b], Huahai Shen [c], Amir Zada [d], Asad Ali [d], Ismail Ahmad [e], Rahim Shah [a], Imran Khan [e], Junsong Chen [f], Chunhua Cui [g], Xiaoqiang Wu [h], Qingquan Kong [h], Jiabao Yi [i], Xiaotao Zu [a], Haiyan Xiao [a,*], Fazal Raziq [a,*], Liang Qiao [a,b,**]

[a] School of Physics, University of Electronic Science and Technology of China, Chengdu 610054, China
[b] Yangtze Delta Region Institute (Huzhou) , University of Electronic Science and Technology of China, Huzhou 313001, China
[c] Institute of Nuclear Physics and Chemistry, China Academy of Engineering Physics, Mianyang 621900, China
[d] Department of Chemistry, Abdul Wali Khan University Mardan, 23200 KPK, Pakistan
[e] Key laboratory of Functional Inorganic Material Chemistry, Ministry of Education of the People's Republic of China, Heilongjiang University, Harbin 150080, China
[f] School of Materials and Energy, University of Electronic Science and Technology of China, Chengdu 610054, Sichuan, China
[g] Institute of Fundamental and Frontier Sciences, University of Electronic Science and Technology of China, Chengdu 610054, China
[h] School of Mechanical Engineering, Chengdu University, Chengdu 610106, China
[i] Global Innovative Centre for Advanced Nanomaterials, School of Engineering, The University of Newcastle, Callaghan, NSW 2308, Australia

ARTICLE INFO

Keywords:
Solar UV-blind β-Ga_2O_3
Metal-phthalocyanines
Photocatalysis
HER
Visible/infrared-light

ABSTRACT

In this work, an efficient wide solar light-driven photocatalyst based on solar UV-blind β-Ga_2O_3 quadrilateral nanorods (β-GOR) has been modified with cobalt phthalocyanine (CoPc). Guided by density functional theory (DFT) calculations and experimental results, H-bond strengthened interfacial connection was established to purchase wide range of solar radiations and applied as an efficient photocatalysts for H_2 evolution from water. The optimized 3CoPc/β-GOR nanocomposite unveiled an unprecedented in the quantum efficiency (0.38%) at 660 nm excitation wavelength with outstanding structural stability compare to the pristine solar UV-blind β-GOR (0%). The much extended photoactivities are accredited to the formation of strong H-bond between CoPc and β-GOR, that accelerated charge transformation as confirmed from Bader charge/work function analysis, activation of O_2, wide visible-light absorption, as well as joint DFT and experimental results. We believe that this system will also work for other metal phthalocyanines such as ZnPc, NiPc and HPc together with β-GOR towards next-generation efficient photocatalysts with wide-visible light response.

1. Introduction

Renewable and clean energy sources (solar, wind, and marine energy) though are copious yet they are seemed to be sporadic and disparity [1,2]. Therefore, the development of energy storage/conversion systems is of prime importance [3–5]. Photocatalytic water splitting, an auspicious technology to convert solar energy into high energy density hydrogen (H_2) fuel with high-output energy and zero carbon emission, has therefore appealed marvelous attention [6,7]. However, for the efficient photocatalytic fuel production, the development of a suitable photocatalyst is one of the recipes for commercial application of this technology [8–10]. Although Pt and Ru/Ir-based oxide materials are the state-of-the-art photocatalysts for water splitting, their applications are quiet restrained by their paucity and high price. Therefore, the development of an efficient and durable water splitting photocatalyst is a precondition for the industrial insinuation of the process.

Among incredible number of materials, gallium oxide (Ga_2O_3) is identified as a wide bandgap material, and exists in different (categorized α, β, γ, δ and ε) polymorphs [11–13]. These characteristic crystal

* Corresponding authors.
** Corresponding author at: School of Physics, University of Electronic Science and Technology of China, Chengdu 610054, China.
E-mail addresses: hyxiao@uestc.edu.cn (H. Xiao), fazal.raziq@uestc.edu.cn (F. Raziq), liang.qiao@uestc.edu.cn (L. Qiao).
[1] Sharafat Ali and Sajjad Ali contribute equally.

https://doi.org/10.1016/j.apcatb.2022.121149
Received 25 September 2021; Received in revised form 16 January 2022; Accepted 24 January 2022
Available online 29 January 2022

structures basically affect the surface properties of Ga_2O_3, leading to the variation in catalytic activity of the polymorphs. Among those polymorphs, β-Ga_2O_3 is an ultra-wide bandgap thermodynamically stable semiconductor, and all the other polymorphs can be ultimately transformed into β-Ga_2O_3 by calcination [14,15]. Due to its ultra-wide bandgap that corresponds to the cut-off wavelength of 260–280 nm, β-Ga_2O_3 is intrinsically solar-blind. β-Ga_2O_3 oxide is famous for water splitting under UV light irradiation and is probable to be more facial than other metal-oxides because its conduction band (CB) position is more negative than other metal-oxides materials [13,16,17]. However, it has been rarely used under visible-light and has not been yet used under near infrared-light, to the best of our knowledge.

Recently, constructing heterojunction has been acknowledged as a prospective avenue to momentously boost the charge separation. Metal oxides, such as TiO_2 [18], Al_2O_3 [19] etc. have been used to couple with β-Ga_2O_3 by several research groups in order to secure magnificent performance for water splitting. Meanwhile, the charge induced reaction proficiency of such metal-oxides/β-Ga_2O_3 heterojunction is comparatively low, and the extension of light response is restricted to UV or UV–vis light region only. Therefore, it is very vital to develop a new heterojunction system with enhanced charge separation and wide visible-light response. Based on the above analyses, coupling β-Ga_2O_3 with other organic semiconductor materials with a matched energy band alignments structure is vital for achieving a good match combination to achieve fast charge separation and wide visible-light absorption. These stimulated us to select metal phthalocyanines (MPc) to construct a traditional-scheme with β-Ga_2O_3, due to their characteristic visible/near-infrared selective absorption regions [20,21] and the matched energy band alignments (the LUMO energy levels of MPc are close to the CB of β-Ga_2O_3. Expectedly, the construction of MPc/β-Ga_2O_3 would both greatly enhance the charge separation and extend the light absorption.

As a member of the MPcs family, Cobalt phthalocyanine (CoPc) has aroused extensive consideration as a member of the MPc family, and majority of the studies focus on the construction with narrow band gap to extent the light absorption [21–23], but no work has been devoted to solar UV-blind semiconductor systems for H_2 production under visible/near-infrared selective absorption regions. Generally speaking, the energy level of the LUMO of CoPc is slightly higher than the CB of β-Ga_2O_3, which is conducive for the sensitization. In fact, based on the energy level positions, CoPc molecule potentially can capture photon energy of visible/near-infrared and inject excited electrons into the CB of β-Ga_2O_3, then the adsorbed O_2 on β-Ga_2O_3 surface can accept electrons to form superoxide. This significantly extends light absorption and promotes the separation of electrons and holes, resulting in greatly improved efficiency for water reduction.

Herein, we have efficaciously constructed the matched energy band alignments MPc/β-GOR heterojunctions by PVA-assisted hydrothermal method and successive heat treatment, and found that the modifier CoPc is much superior than ZnPc, NiPc and HPc for photocatalytic H_2 production. The optimized CoPc/β-GOR heterojunction unveiled unprecedented sonophotocatalytic activity, produced H_2 (110 μmolg^{-1}), confirming the structure stability of the heterojunction. This unprecedented sonophotocatalytic activity is primarily accredited to ultrasonic waves, O_2 promotion, and wide vis-light absorption guidance by experimental and DFT results. This work unlocks new potentials to solar blind β-GOR for proficiently photocatalytic water reduction by coupling with MPc, and the established approach of modifying MPc is also valid to other solar UV-blind semiconducting photocatalysts.

2. Experimental section

2.1. Synthesis of β-Ga_2O_3 quadrilateral nanorods (β-GOR)

All the substances (obtained from Beijing Chemical Co., Ltd.) were analytical pure and original.

Hydrothermal method was employed to synthesized quadrilateral nanorods of β-GOR. In a classic experiment, 4 g (5 mmol) Ga$(NO_3)_3$·xH_2O and 0.2346 g PVA were dissolved in 40 mL deionized water. After heating in a circulator at 90°C for 15 min, the mixture was transferred to a 25 mL Teflon-lined stainless steel autoclave and kept for 8 h at 200 °C. Afterward, the white precipitates were obtained through by centrifugation, and rinsed several times with deionized water and ethanol and dried in oven at 80 °C. Finally, the quadrilateral nanorods of β-GOR was obtained from the dried precipitates via calcination for 2 h at 700 °C under N_2 atmosphere (heating rate of 1 °C/min).

2.2. Synthesis of CoPc/β-GOR nanocomposite (xCoPc/β-GOR)

1 g β-GOR was dispersed in 30 mL ethanol under ultrasonication for 30 min. A calculated volume of CoPc solution in ethanol was added to the β-GOR suspension followed by sonication and stirring for 30 min to obtain a homogenous suspension. It was further stirred at room temperature for 6 h and the solvent was then evaporated under stirring at 80 °C and finally dried at 80 °C overnight. In this way, different mass ratio (1%, 2%, 3% and 4%) of CoPc to β-GOR were prepared and represented by xCoPc/β-GOR, where x indicates the mass ratio of CoPc to β-GOR. For comparison, we also loaded 3% by mass of other metals phthalocyanines (HPc, ZnPc, and NiPc) to β-GOR to prepare 3HPc/β-GOR, 3ZnPc/β-GOR, and 3NiPc/β-GOR nanocomposites respectively.

2.3. Sample characterization

An X-ray diffractometer (XRD) (D/max-2400, Rigaku, Japan) was used to describe the crystal structure. The optical properties were measured using UV–vis diffuse reflectance spectra (Model Shimadzu UV2550 spectrophotometer). The surface area was analyzed by Brunauer-Emmett-Teller (BET) (ASAP2020Plus 1.03 apparatus). Fourier-transform infrared (FT-IR) spectra was made by an infrared spectrophotometer (Nicolet Is-10 model, USA) by adopting the KBr technique. Morphology and chemical composition were explored by scanning electron microscopy (FE-SEM, EM-8000, KYKY, China) and transmission electron microscopic (TEM, JEOL JEM2100 (RH)), correspondingly. The chemical state of the nanocomposites was measured by X-ray photoelectron spectroscopy (XPS) (Escalab 250Xi).

2.4. Analysis of hydroxyl radicals

0.05 g sample were well-dispersed in 70 mL aqueous coumarin solution (0.001 mol L^{-1}) in a beaker. Before subjected to irradiation, the beaker was magnetically stirred for 20 min to attain to get coumarin particle adsorb on the surface of the photocatalyst. After 2 h irradiation, a specific amount of the sample was taken for the fluorescence test of 7-hydroxycoumarin with excitation wavelength (332 nm) and an emission wavelength (460 nm) via a spectrofluorometer (Perkin-Elmer LS 55).

2.5. Evaluation for O_2 temperature-programmed desorption (O_2-TPD)

50 mg sample were preheated in a self-build apparatus for 0.5 h at 300 °C to eliminate any humidity. The system was cooled to room temperature under an ultra high pure He gas and then applied O_2 for 1 h at 30 °C. The surface weakly adsorbed O_2 was detached by subjection to ultra high pure He. The temperature was then raised to 500 °C (10 °C min^{-1}) under pure He.

2.6. Photoelectrochemical (PEC) and electrochemical (EC) experiments

Photoelectrochemical (PEC) and electrochemical (EC) reduction measurements were made in a conventional 3 electrode system. The as-prepared nanocomposite was employed as a working electrode, platinum plate (99.9%) as counter electrode and saturated KCl Ag/AgCl electrode as reference electrode in 0.5 mol L-1 Na_2SO_4 electrolyte

solution. High pureness N_2 gas (99.999%) was bubbled over the electrolyte before and during the experiments. The PEC experiment was performed out in a quartz tank, using a 300 W xenon lamp and a cut-off filter $\lambda \geq 420$ nm as a light source. The photoelectrochemical and electrochemical properties of a series of catalysts were tested by IVIUM V13806 electrochemical workstation.

2.7. EPR measurements

Since $\bullet O_2^-$ radicals are trapped by 5,5-dimethyl-L-pyrroline N-oxide (DMPO) producing the EPR signals, 5 mg sample were dissolved in DMPO and diluted with CH_3OH to obtain a liquid mixture. After illumination, the mixture was characterized using a Brucker EPR 300E spectrometer (298 K).

2.8. Photocatalytic experiments for H_2 evolution

The photocatalytic H_2 evolution experiments were arranged in a sealed Pyrex top-irradiation reaction vessel fitted with a glass closed gas circulation system. In general, the 50 mg photocatalyst was distributed in 80 mL water and 20 mL methanol (sacrificial agent) mixed solvent. The sealed reaction system was degassed for about 30 min before irradiation to completely evacuate the air in the system and irradiated under vis-light ($\lambda \geq 420$ nm) by means of a 300 W Xenon-lamp. During the reaction, the system is connected to the circulating cooling water machine to keep the system temperature at 12 °C. In order to detect the gas generated after photocatalytic reaction, an on-line gas chromatograph with thermal conductivity detector (TCD) is equipped in the reaction system with Ar as the carrier gas. For the photocatalytic recoverability test, the experiment was carried out under the same experimental conditions and retested for 5 cycles each of 4 h each. After each cycle, turn off the xenon lamp, empty the air in the reaction system and start the next cycle.

2.9. Computational setup

In current study density functional theory (DFT) calculations have been performed using generalized gradient approximation (GGA) in the form of Perdew-Burke-Ernzerhof (PBE) [24] functional for the exchange-correlation potentials as implemented in the Vienna ab initio simulation package (VASP), with consideration of spin-polarization [25–27]. A 2 × 3 × 1 k-points and 450 eV energy cutoff have been used to optimized structures. To describe van der Waals corrections in DFT calculations, we included DFT-D3 correction method of Grimme [28]. The current simulation was carried out for 2 × 3 supercell β-Ga_2O_3 (1 0 0) surfaces with 64 Ga atoms and 96 O atoms, respectively. The β-Ga_2O_3 supercell is orthorhombic 12.14 × 11.59 × 25.04 $Å^3$ for x, y, and z-direction, with $\alpha = \beta = \gamma = 90^\circ$ and the periodic condition is employed along x and y directions. periodic Co-Phthalocyanine with 32 C atoms, 8 nitrogen atoms and 1 Co atoms is place on the surface of β-Ga_2O_3. The vacuum thickness was set to be ~ 13 Å in the z-direction to minimize the interaction between periodic interlayer. The total energy was converged to an accuracy of 1×10^{-5} eV to obtain accurate forces, and a force tolerance of 0.02 eV/Å was applied in the structure optimization. The energies of gas-phase H_2 molecule was calculated in a box in the size of 27 Å × 27 Å × 20 Å.

The binding energies of CoPc/β-Ga_2O_3 interface were calculated using the formula.

$$E_b = E_{CoPc/\ \beta\text{-}Ga2O3} - E_{\beta\text{-}Ga2O3} - E_{CoPc} \quad (1)$$

where $E_{CoPc/\ \beta\text{-}Ga2O3}$, $E_{\beta\text{-}Ga2O3}$, and E_{CoPc} represent the energies of the interface, the isolated β-Ga_2O_3 surface, and isolated monolayer CoPc, respectively.

Bader charge calculation was performed to analyze the charge population and charge transfer [29,30].

$$\text{work function} = \text{Vacuum potential } (E_{vac}) - \text{Fermi level } (E_F) \quad (2)$$

The charge density difference Δρ was calculated as.

$$\Delta\rho = \rho_{CoPc/\beta\text{-}Ga2O3} - \rho_{\beta\text{-}Ga2O3} - \rho_{CoPc} \quad (3)$$

where $\Delta\rho_{CoPc/\ \beta\text{-}Ga2O3}$, $\rho_{\beta\text{-}Ga2O3}$, and ρ_{CoPc} represent the charge densities, of CoPc/β-Ga_2O_3, the isolated β-Ga_2O_3 surface, and isolated monolayer CoPc, respectively.

The work function is calculated was calculated using the formulation.

We considered CO_2RR to CO that proceeds through two-electron transfer mechanism, and included two proton-electron coupled elementary steps:

$$H^+ + e^- + * \rightarrow H^* \quad (4)$$

$$H^* + H^+ + e^- + * \rightarrow H_{2(g)} \quad (5)$$

where "* " denoted the active site of catalysts, (g) denoted gas phase, respectively, and H^* are the adsorbed intermediate.

The zero-point energy, entropy, and enthalpy corrections were added to adsorbates to convert electronic energy to free energy.

The Gibbs free energy (G) at 0 V is modified by Eq. (6).

$$G = E_{DFT} + E_{ZPE} - TS + \int C_p dT \quad (6)$$

where E_{DFT}, E_{ZPE}, TS, and $\int C_p dT$ denote electronic energy obtained from DFT optimization, zero-point vibrational energy, entropy, and heat capacity at room temperature (T = 298.15 K). The computational hydrogen electrode (CHE) model was used to calculate the Gibbs free energy for the reaction step involving the coupled proton-electron, in which the free energy of a pair of proton and electron ($H^+ + e^-$) was calculated as a function of applied potential relative to a reversible hydrogen electrode (U vs RHE), i.e., $\mu(H^+) + \mu(e^-) = \frac{1}{2}\mu(H_2) - eU$ [31]. The adsorption free energies of H^* at a given potential U_{RHE} can be calculated as:

$$\Delta(H*) = G(H*) - G(*) - \frac{1G(H2)}{2} - eU_{RHE} \quad (7)$$

3. Results and discussion

3.1. Structural and performance comparison of different MPc modified β-GOR

The synthetic procedure for loading metal phthalocyanines on the surface of β-Ga_2O_3 quadrilateral nanorods (MPc/β-GOR) is illustrated in Scheme 1. β-GOR was synthesized by a PVA-assisted hydrothermal and succeeding heat treatment method. The MPc/β-GOR heterojunction was constructed by loading polymeric MPc on the β-GOR surface through sol-gel method. The XRD patterns of β-GOR and 3MPc/β-GOR are well consigned with high purity, and there are no peaks related to MPc because of its low amount and high dispersion as illustrated in Fig. S1a [32]. However, the UV/Vis diffuse reflectance spectra (DRS) indicate the momentous shifting of the absorption band of β-GOR to longer wavelength side, which perceptibly indicates that β-GOR is successfully modified with MPc (Fig. S1b). As the activation of O_2 is a powerful tool for charge separation, therefore, its adsorption capacity on the surface of metal sites was first revealed by theoretical calculations as illustrated in Fig. 1a. The O-O bond distance of adsorbed O_2 is elongated from 1.23 (gas phase) to 1.3 Å, and the adsorption energy of O_2 on 3CoPc/β-GOR (−1.19 eV) surface is higher than 3ZnPc/β-GOR (−0.41 eV), 3NiPc/β-GOR (−0.35 eV), 3HPc/β-GOR (−0.26 eV) and β-GOR (−0.21 eV), which is further supported by the O_2 temperature-program desorption (O_2-TPD) curves (Fig. 1b). It is customarily acknowledged that the amount of formed hydroxyl radicals (•OH) reflects the charges separation form during photocatalysis. Thus, it is prime to evaluate the •OH amount formed during the photochemical reaction to validate

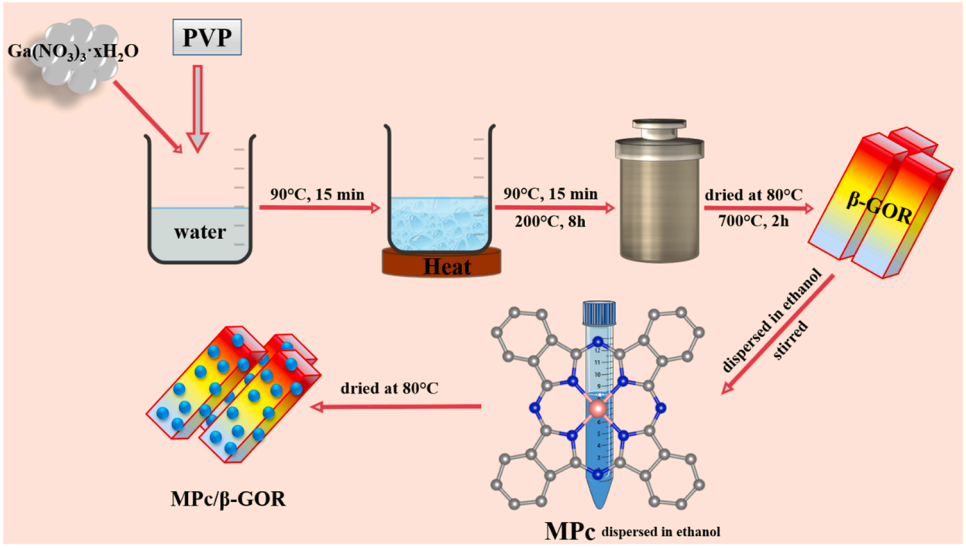

Scheme 1. Schematic illustration of the formation of quadrilateral nanorods β-GOR composite.

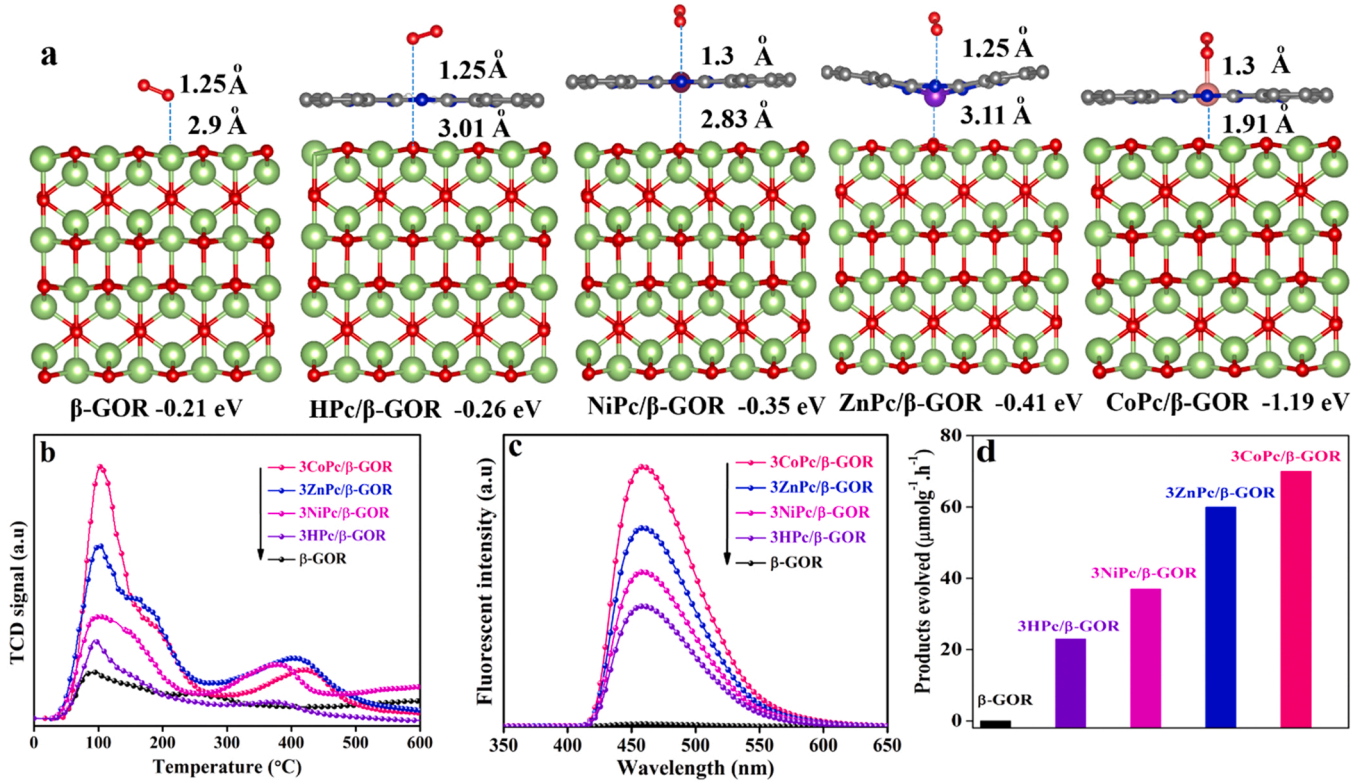

Fig. 1. The optimized structures with corresponding bond distance (Å) and adsorption energy (eV) of (a) O_2 on the surface, O_2-TPD curves (b), FS spectra related to the amount of (c) •OH radicals, and photocatalytic activities for H_2 evolution under visible-light irradiation of (d) β-GOR and 3MPc/β-GOR (M=Co, Zn, Ni and H, x means represents the mass ratio percentage of MPc to β-GOR and β-GOR means β-Ga_2O_3).

charge separation. The coumarin fluorescent (FS) method is generally used to probe the produced •OH amounts, meanwhile the coumarin effortlessly reacts to form luminescent 7-hydroxy-coumarin. The fluorescence intensity of 7-hydroxy-coumarin is therefore is directly associated with the amount of produced •OH. The stronger fluorescence intensity means higher •OH amounts and vice versa [7,33,34]. In Fig. 1c, it is noticed that all the 3MPc/β-GOR samples deliver stronger FS responses than the virgin β-GOR, and the response of 3CoPc/β-GOR is the strongest, indicating its perceptibly enhanced charge separation. Besides, electrochemical curves (Fig. S2), electrochemical impedance spectra (EIS) results (Fig. S3), and photoelectrochemical I-V curves (PEC I-V) (Fig. S4), reflect coincident results. One can see that the superiority of the charge separation of 3MPc/β-GOR becomes significant. The photoactivity of all the investigated 3MPc/β-GOR nanocomposites are found to be proportional to the charge separation, and display much higher H_2 evolution than virgin β-GOR under visible-light, and the CoPc-modified one is the best one (Fig. 1d). The photocatalytic activity of virgin β-GOR and different 3MPc/β-GOR were also investigated at 660 nm excitation wavelength (Fig. S5), and the CoPc-modified sample displays best photoactivities, confirming that light absorption of β-GOR

is greatly extended to visible-light/near infrared region by the loaded MPc. Hence, 3CoPc/β-GOR heterojunction is selected as a characteristic case to explore the fabricated MPc/β-GOR system in details.

3.2. Effects of CoPc modifier on the structural and performance on β-GOR

Fig. S6 illustrates the XRD patterns of hydrothermally and sol-gel prepared photocatalysts. All the peaks can be well indexed with no impurity peaks. Also the corresponding XRD peak of CoPc is not detected in the patterns of xCoPC/β-GOR, due to its excellent adsorption and well dispersion on the surface of β-GOR instead of being aggregated. The DRS spectra were used to regulate the light absorption properties of the β-GOR and xCoPC/β-GOR. The absorption spectrum of xCoPC/β-GOR reveals two main bands; Soret band at 300–360 nm and a Q band at 600–750 nm (Fig. 2a). The DRS spectra noticeably display that the typical absorption of xCoPC/β-GOR is steadily extended with increase in the amount of introduced CoPc, demonstrating that the polymeric CoPc is efficaciously loaded on the surface of β-GOR. The interfacial bonding mode of β-GOR and CoPc were confirmed by FTIR spectra as illustrated in Fig. 2b. The peak intensity of surface hydroxyl groups at 1630 cm^{-1} of β-GOR is weakened after the introduction of CoPc, signifying CoPc

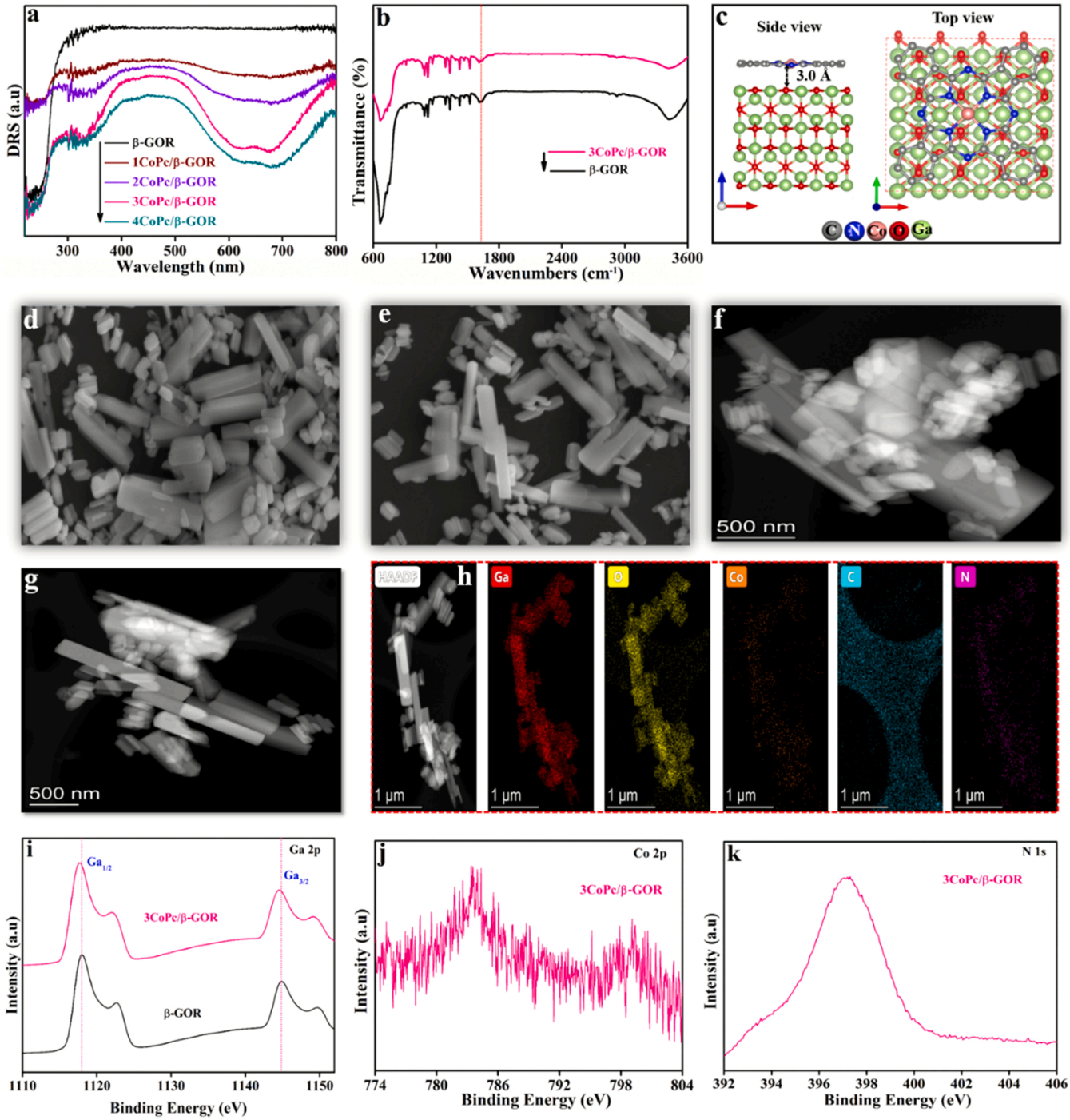

Fig. 2. DRS spectra of β-GOR and xCoPc/β-GOR (a), FTIR spectra of β-GOR and 3CoPc/β-GOR (b), DFT optimized CoPc/β-GOR structure and the strong bonding interaction between surface hydroxylated β-GOR and CoPc (c), SEM (d, e) and TEM of β-GOR and 3CoPc/β-GOR respectively (f, g), EDX of 3CoPc/β-GOR (h), XPS spectra for Ga 2p of β-GOR and 3CoPc/β-GOR (i), Co 2p for 3CoPc/β-GOR (j) and N1s for 3CoPc/β-GOR (k).

connection with the surface hydroxyl groups of β-GOR [35]. The density functional theory (DFT) calculations further endorse the experimental results of the powerful interaction between CoPc and β-GOR after the stable adsorption structure optimization. Accordingly, it is suggested that the hydrogen bond is formed with equilibrium distance of ~ 3.0 Å (Fig. 2c) between N atom of CoPc and hydroxyl groups of β-GOR, and their binding energy is ~ − 2.4 eV (Fig. S7), implying the favorable charge transfer and separation.

The Brunauer-Emmett-Teller (BET) results show that the specific surface areas of the as-obtained β-GOR, 1CoPc/β-GOR, 2CoPc/β-GOR, 3CoPc/β-GOR and 4CoPc/β-GOR nanocomposites are around 4.82, 6.56, 7.51, 12.4 and 10.5 $m^2. g^{-1}$, respectively (Fig. S8). It is clear that 3CoPc/β-GOR offers more active adsorption sites leading to more efficient photocatalysis. The structures and morphologies of β-GOR and 3CoPc/β-GOR nanocomposites were further characterized by scanning electron microscopy (SEM), transmission electron microscopy (TEM), selected area electron diffraction (SAED) and energy-dispersive X-ray (EDS/EDX) as illustrated in Fig. 2. The SEM image of β-GOR (Fig. 2d), discloses the quadrilateral nanorods like morphology with average length and width as 1.22 μm and 0.23 μm respectively. After CoPc introduction (Fig. 2e),

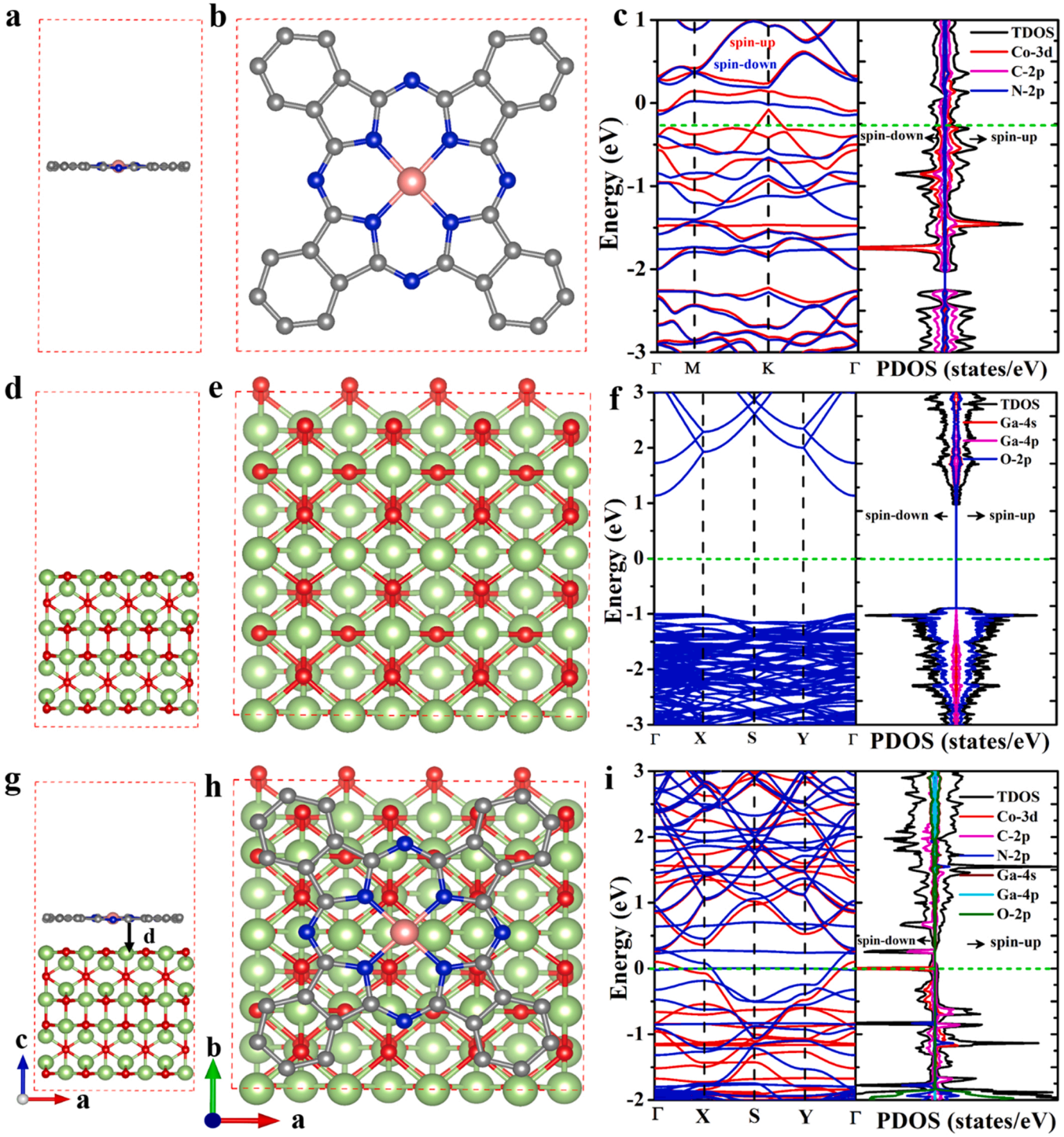

Fig. 3. The electronic band structure, spin-polarized total density of states (TDOS), and partial density of states (PDOS) plotted together with corresponding optimized structures with side and top view of pure CoPc (a-c), pure β-Ga_2O_3 (d-f), and CoPc/β-Ga_2O_3 (g-i) respectively.

the quadrilateral nanorods grow in length to 1.10 μm and shrink in width to 0.20 μm. From these observations, it is confirmed that the support plays a major role in providing high surface area to the catalysts for efficient photocatalysis. TEM image further confirms the quadrilateral nanorods structure of β-GOR (Fig. 2f) and 3CoPc/β-GOR nanocomposites (Fig. 2g), HRTEM of the amount-optimized 3CoPc/β-GOR was measured, and its confirm that CoPc is successfully modified with β-GOR as illustrated in Fig. S9, and the single crystalline nature of the quadrilateral nanorods is confirmed by selected area electron diffraction (SAED) patterns illustrated in Fig. S10a and b of β-GOR and 3CoPc/β-GOR respectively. TEM-based energy-dispersive X-ray (EDX) analysis was carried out to analyze the elemental composition and distribution of β-GOR (Fig. S11) and 3CoPc/β-GOR (Fig. 2h and Fig. S12). The EDX mapping of β-GOR reveals a homogeneous distribution of C, Ga and O, and the heterojunction 3CoPc/β-GOR reveals a homogeneous distribution of C, Co, N, Ga and O, which unambiguously demonstrates that CoPc is uniformly distributed on the surface of β-GOR. XPS was performed to investigate the oxidation state and chemical compositions of the samples. It is found that the peaks of Ga 2p (Fig. 2i), and O1s (Fig. S13) in 3CoPc/β-GOR are slightly shifted toward lower binding energy compare to the β-GOR. This indicates that the charge densities increase in β-GOR and decrease in CoPc as a result of the electronic redistribution after their coupling to form effective heterojunctions. The peak of C1s (Fig. S14) is found around at 284.5 eV [36], while that of Co2p at 782.1 eV ($p_{1/2}$) and 797.7 eV ($p_{3/2}$) [37], and N1s at 397.15 eV [38] respectively in Fig. 2j and k, confirming that CoPc is present in the nanocomposite.

The geometry and electronic properties of the as-prepared samples were further studied by DFT as illustrated in Fig. 3. The band structure and projected density of states (PDOS) indicate that CoPc shows a metallic behavior with band dispersion across the Fermi level (E_F) (Fig. 3a-c). However, β-GOR (Fig. 3d-f) shows semiconducting behavior with a band gap of 2.5 eV as calculated from DFT-D3, and 4.9 eV measured using HSE, LDA+GW previous study [39,40]. The fully optimized structure of CoPc/β-GOR is illustrated in (Fig. 3g-i), which governs a stable orthorhombic structure and metallic behavior with optimized lattice parameters a = 12.14 Å, b = 11.59 Å, and c = 25.04 Å. The density of states calculation reveals that Co d and C p-orbitals hybridize with p-orbitals of surrounding O atoms around the Fermi level (E_F) providing metallic characteristic to CoPc/β-GOR.

Besides, the wide-light absorption, the charge separation is the primary dynamics figuring out the efficiency of photocatalysis. Lifetime of

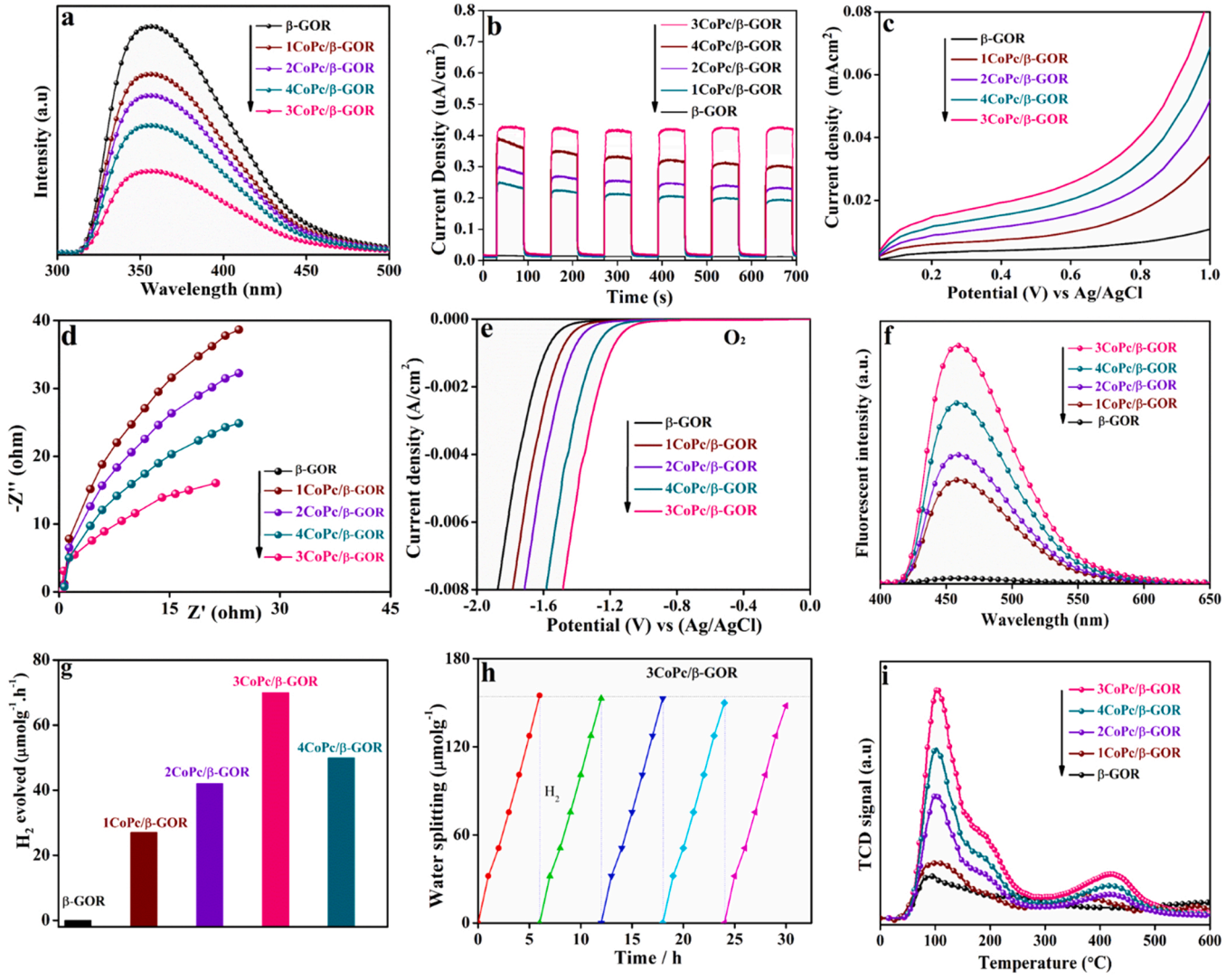

Fig. 4. Photoluminescence of β-GOR and xCoPc/β-GOR (a), transient photocurrent density of 3CoPc/β-GOR (b), PEC I-V curves (c), EIS Nyquist plots in light (d) Electrochemical reduction curves in O_2 (e), FS spectra related to the amount of •OH radicals (f), and photoactivity of β-GOR and xCoPc/β-GOR (g), stability test of xCoPc/β-GOR for H_2 evolution (h), and O_2-TPD of β-GOR and xCoPc/β-GOR (i). Here x represents the mass ratio percentage of CoPc to β-GOR and β-GOR means β-Ga_2O_3.

photogenerated charge carriers was confirmed by photoluminescence spectroscopy (PL) analysis as illustrated in Fig. 4a. The strong PL intensity reflects a high recombination rate of photoinduced charges and vice versa. Obviously, the optimized 3CoPc/β-GOR nanocomposite has momentously low PL emission. This outcome suggests that the constructed heterojunction between β-GOR and CoPc is efficient to retard charge recombination, and is consistent with the observed photoactivity [7,41,42]. A similar propensity is also registered in the transient photocurrent density under visible-light irradiation (Fig. 4b). It can be seen that all of the photoelectrodes show distinctive open circuit potentials. Undoubtedly, the 3CoPc/β-GOR shows higher photovoltage. The open circuit potential of amount-optimized 3CoPc/β-GOR increases abruptly when light is on and decreases rapidly when light is off, suggesting efficient charge separation in 3CoPc/β-GOR. The electrochemical (EC) results under N_2 (Fig. S15) and O_2 environments (Fig. 4c), photoelectrochemical I-V curves under visible-light irradiation (Fig. 4d), EIS under dark (Fig. S16) and vis-light (Fig. 4e), and FL spectra (Fig. 4f) further demonstrates enhanced charge separation in the as-prepared nanocomposites with highest charge separation in the optimized 3CoPc/β-GOR. The photocatalytic activities for H_2 evolution were assessed under vis-light and also at 660 nm excitations wavelength. One can see that the photocatalytic activity of β-GOR is significantly improved after introducing CoPc, and the optimized 3CoPc/β-GOR composite delivers nearly 70-time improved activity than the virgin β-GOR (Fig. 4g). Even though the H_2 evolution activity of 3CoPc/β-GOR at 660 nm (Fig. S17) and at 700 nm and 800 nm (Fig. S18) is significant highlighting the role of loaded CoPc. Interestingly, the optimized 3CoPc/β-GOR sample also produced about 0.15 μmol g^{-1} h^{-1} H_2 gas up to 750 nm excitation wavelength. However, further increase in the wavelength up to 800 nm could not produce appreciable amount of H_2 gas which is related to the very low amount of energy possessed by these photons to separate H_2 from water. The low energy photons are unable to produce excited charges for the reduction of the water molecules to generate H_2 gas. Based on theoretical and experimental results, these unprecedented activities of the optimized nanocomposite can be attributed to the formation of H-bond between CoPc and β-GOR, that facilitates charge transformation as confirmed by Bader analysis, O_2 activation, and wide visible-light light absorption. The cycling stability, a critical necessity in practical application of water reduction, was measured as illustrated in Fig. 4h. The H_2 evolution over 3CoPc/β-GOR shows obviously no change after 20 h photoreduction test with a 5 h run cycle, validating its auspicious photostability [43] (Fig. 4**i).** To further recognize its superiority, we have evaluated the durability performance of 3CoPc/β-GOR for H_2 evolution as illustrated in Fig. S19. Durability is the ability of a material to show activity for a long time without significant deterioration and requiring minimum maintenance. It is an important factor in assessing the sustainability of a material. We have measured the durability of the amount-optimized 3CoPc/β-GOR for continuously 30 h. Our sample shown outstanding photoactivity for H_2 evolution (710 μmol g^{-1} h^{-1}). It is seen that no detectable change is observed in the H_2 evolution efficiency even after 30 h. Consequently, 3CoPc/β-GOR can be considered as stable photocatalyst for practical applications".

To support the above results, we conducted O_2 temperature-program desorption (O_2-TPD) experiment. It is certainly assumed that the adsorption of O_2 is critical for photocatalysis meanwhile the adsorbed O_2 might excellently trap the photogenerated electrons to form super oxide anions (Fig. 4j). Since the extended pi network of CoPc is vastly favorable for adsorption of O_2 molecules through p-p interactions, 3CoPc/β-GOR presents a much larger adsorbed amount of O_2 molecules than those by the pristine β-GOR.

4. Discussion

To get a deeper insight into the HER on CoPc/β-Ga_2O_3 material, we have conducted DFT calculations as summarized in Table S1. The scheme, active sites, and free-energy reaction pathways at 0 V vs. RHE is shown in Fig. 5a and b. Our calculation revealed that ΔG of the two elementary steps of HER on CoPc/β-GOR, i.e., $H^* + H^+ + e^- \rightarrow H_2$, namely the Heyrovsky reaction is the potential determining step of the HER [44]. The over-potentials required for HER on Co, C, N, N-edge, O, and Ga-sites are 0.23, 0.96, 0.79, − 0.79, − 0.37, and − 0.72 eV respectively.

Therefore, after verified the improved photoactivity, it is still crucial to firmly clarify the interfacial charge transfer mode in the constructed nanocomposites. The monochromatic photocurrent action spectra were measured and illustrated in Fig. 6a. In addition, the photocurrent response of 3CoPc/β-GOR is undoubtedly perceived even under 660 nm excitation, resulting in the transfer of electrons from CoPc to β-GOR under vis-light radiation. To further confirm this result, the FS spectra related to the amount of produced hydroxyl radicals were obtained under different wavelength monochromatic light excitations (Fig. S20). In addition, photocatalytic activity of H_2 evolution with monochromatic light excitation were performed to illuminate the contribution properties (Fig. 6b). It is discerned that the photoactivity of 3CoPc/β-GOR at 420 nm light excitations is much higher than that of 660 nm. In the meantime, the quantum efficiency is also calculated at 420 and 660 nm, which is approximately 7-time higher at 420 nm excitation than at 660 nm, asserting that the light excitation begins at 420 nm and extends up to 660 nm to endow enough thermodynamic energy for the photo-induced electrons to understand the interfacial charge transfer from CoPc to β-GOR, meanwhile the CoPc energy level is slightly higher than the CB of β-GOR. To further confirm the above reactions, the quantum efficiency and absorption spectrum were carried out for pure β-GOR and 3CoPc/β-GOR under excitation by Xeon lamp light with cut off-wavelengths of 420 nm, 500 nm, 660 nm, 750 nm and 800 nm in order to analyze quantum efficiency of the reaction as a function of incident light wavelengths as illustrated in Fig. S21. As can be seen from the Fig. S21, since β-GOR shows no absorption in the range of 400–800 nm, therefore, its activities or QE is close to zero. In contrast, as shown in the revised Fig. S21, the amount optimized 3CoPc/β-GOR shows broad absorption peak between 500 and 800 nm, therefore its activity and hence QE is appreciable (much larger than that for β-GOR). These results harmonize well with the photoelectrochemical results mentioned above, demonstrating that CoPc is well suited for extended vis-light response and subsequent charge separation. The low-level electron paramagnetic resonance (EPR) method was used to test the precise electron transfer process at 3CoPc/β-GOR heterojunction. The typical signal of free electrons in the 3CoPc/β-GOR system at g= 1.93 is sensed under dark and the signal intensity displays an apparent enhancement under 420 nm excitation (Fig. 6c). Moreover, the EPR spectra of 3CoPc/β-GOR heterojunction under 660 nm excitation is also measured Fig. 6d. Fascinatingly, there is no perceptible change of EPR signals under 420 or 660 nm excitation. However, the peak intensity for 420 nm is much stronger than 660 nm. This improvement of the peak signal intensity demonstrates that more free electrons are created in the 3CoPc/β-GOR system due to high energy photons. This provides a strong confirmation for the transfer of electrons to β-GOR from CoPc and stored therein.

Besides, in order to determine the charge transformation between CoPc and β-GOR, we calculated the work function of each material separately which is a fundamental surface parameter to determine how effortlessly electrons can be removed to a field-free region outside the surface. The DFT calculated work function of CoPc is 4.93 eV (Fig. 7a) which is lower than that of β-GOR (5.88 eV) (Fig. 7b), it indicates that the electron will transfer from CoPc to β-GOR according to their work functions difference. The Bader charge analysis further proved that 1.7 | e| electron is transferred from CoPc to β-GOR which is consistent with the charge density difference plot illustrated in (Fig. 7c). Based on the above results and discussion, the schematic diagram of photoinduced charge transfer and separation in the 3CoPc/β-GOR nanocomposite and photochemical processes are proposed, as illustrated in Fig. 7d. CoPc be

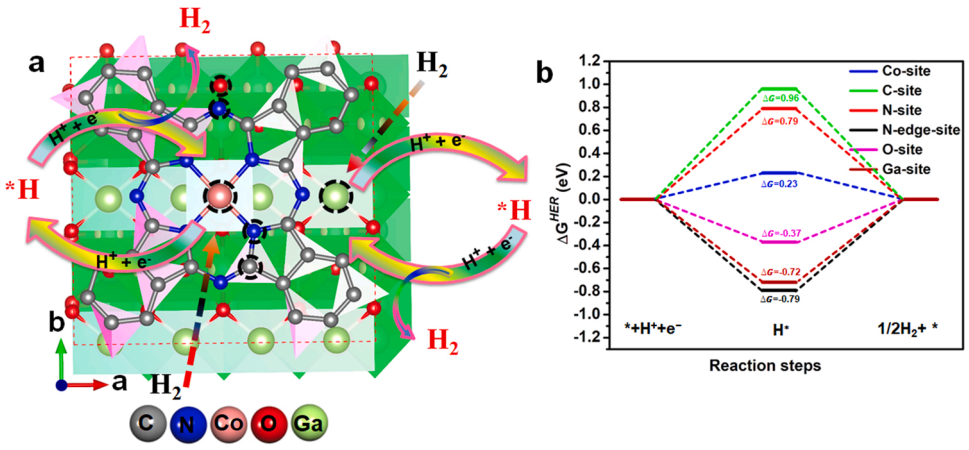

Fig. 5. The scheme (a) and free energy diagrams of HER (b) on the surface CoPc/β-Ga_2O_3 respectively at zero voltage vs reversible hydrogen electrode (RHE) respectively. The black dotted circle in structure "a" represents the active sites for HER.

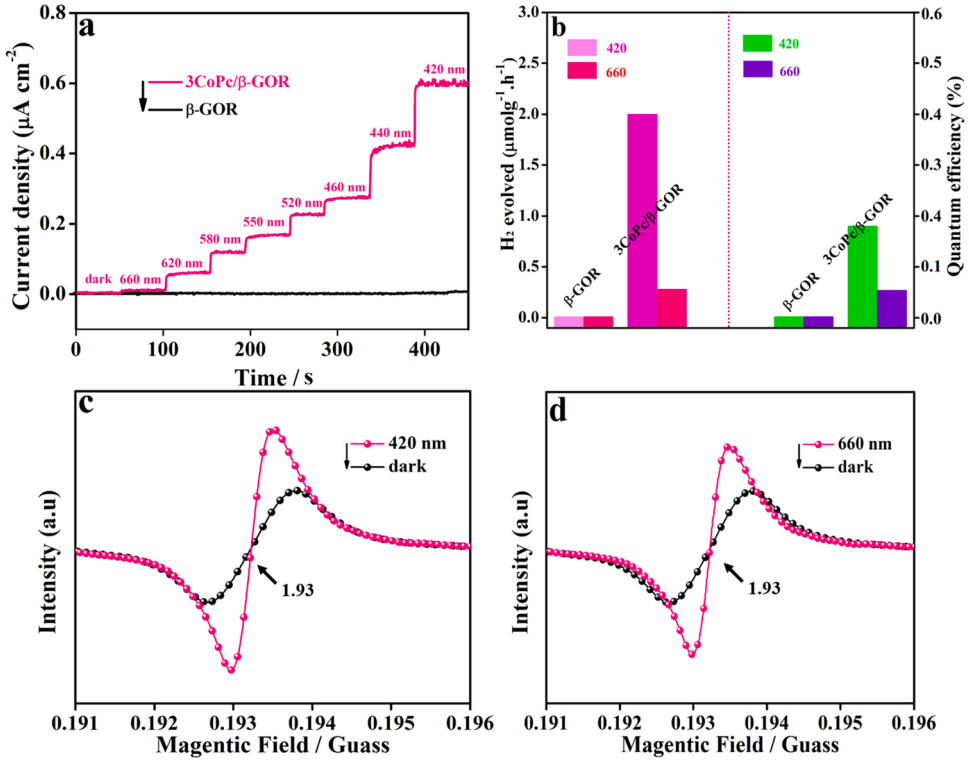

Fig. 6. Photocurrent action spectra of β-GOR and 3CoPc/β-GOR (a), photocatalytic activities for H_2 evolution and the corresponding QE under monochromatic beams (at 420 and 660 nm) for 3CoPc/β-GOR (b) and EPR of 3CoPc/β-GOR under 420 nm (c) and under 660 nm (d).

able to be excited by vis-light to generate electron-hole pairs. β-GOR then assists as an electron capture and proscribes the recombination of hole-electron. Moreover, CoPc promptly transfers excited electrons to β-GOR and improves the separation of holes and electrons, meaningfully endorsing photoefficiency and more importantly greatly extended the light response of β-GOR. As illustrated in Fig. 7e, the as-prepared CoPc/β-GOR heterojunction displays about 110-fold higher sonophotoactivities for H_2 evolution than virgin β-GOR under vis-light irradiation, and there is no change in the XRD and SEM after reaction, further confirming the outstanding stability and widely application. In order to further confirming the wide application of the as-prepared nanocomposites, we have examined the degradation of methanol under vis-light irradiation on 3CoPc/β-GOR for H_2 and CO_2 generation. After 3 h light irradiation, the as-prepared 3CoPc/β-GOR nanocomposite generated H_2 (178 μmol g^{-1}) and CO_2 (19.95 μmol g^{-1}) as illustrated in Fig. S22. Consequently, the DFT and experimental results undoubtedly validate the auspicious potential for proficiently photocatalytic H_2 evolution on the formed MPc/β-GOR heterojunction. Impressively, the CoPc-coupled one demonstrations the outstanding photocatalytic activity, primarily owing to its appropriate energy band position with β-GOR, preferable activation capacity for O_2 and wide solar light absorption.

5. Conclusion

Herein, we have effectually fabricated the matched energy band aligned metal phthalocyanine/ β-gallium oxide nanorods (MPc/β-GOR) heterojunction by a PVA-assisted hydrothermal process and successive heat treatment. The modifier CoPc is much better than ZnPc, NiPc and

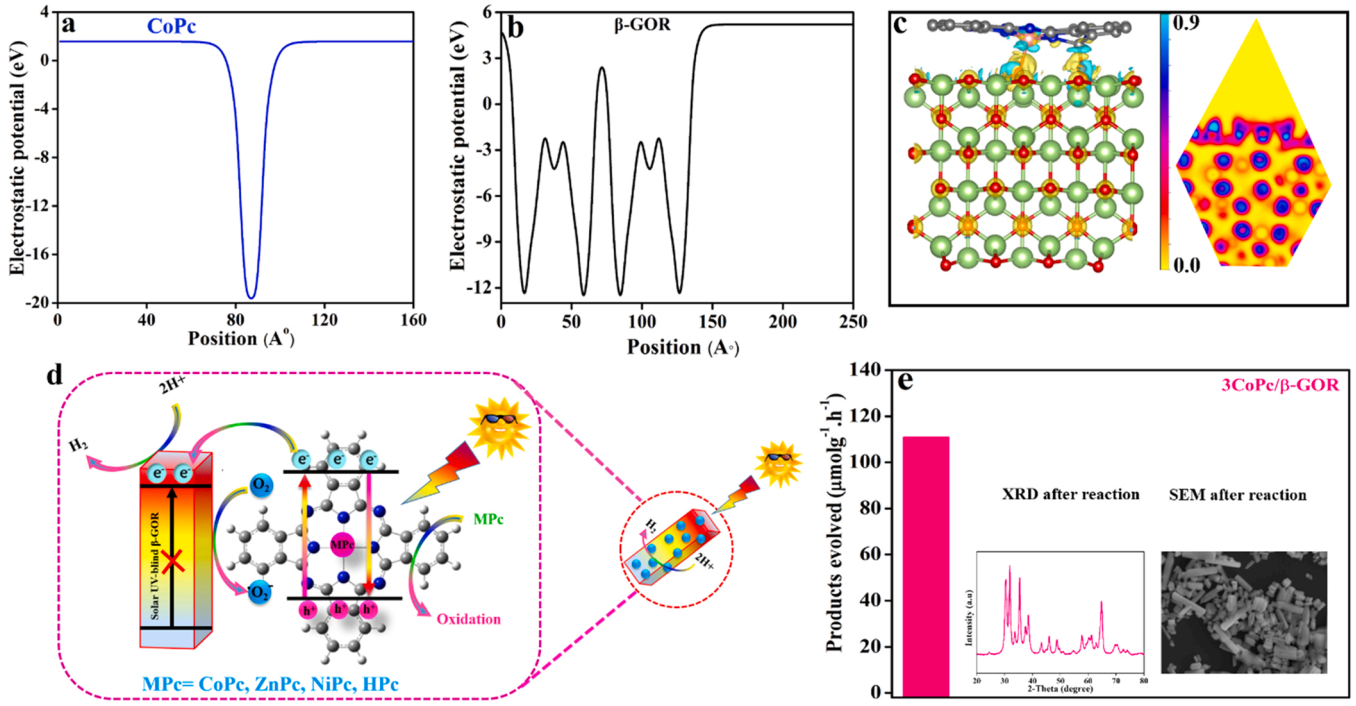

Fig. 7. Work function of pure CoPc (a) and pure β-GOR (b), the charge density difference and electron localization function of CoPc/β-GOR (c), proposed mechanism of 3CoPc/β-GOR (d), and sonophotocatalytic activity of 3CoPc/β-GOR for H_2 evolution with inset XRD and SEM after reaction (e).

HPc for photocatalytic H_2 production. Guided by the DFT calculations, the obtained results reveal that there are strong chemical connections between β-GOR and MPc by the strengthened H-bond formation via the hydroxyl groups of β-GOR connected to the N atoms in the MPc ligand, which keeps the modified MPc vastly dispersed on β-GOR. It is obviously validated that the as-prepared amount-optimized 3CoPc/β-GOR exhibits unprecedented photocatalytic activity for H_2 evolution (110 μmol. $g^{-1}h^{-1}$) under vis-light irradiation, along with calculated quantum efficiencies of 0.38% at 660 nm wavelength. This high photocatalytic activity of the optimized heterojunction is mainly dependent on the suitable energy band position of β-GOR and MPc, and preferable activation capacity for O_2. Moreover, it is suggested mainly on the recyclability test and sonophotoactivity that the heterojunction has outstanding stability. This pioneer scientific work is believed to be feasible for other MPcs such as ZnPc, NiPc and HPc, together with β-GOR.

CRediT authorship contribution statement

Sharafat Ali: Data curation, Writing – original draft. **Sajjad Ali, Haiyan Xiao**: Theoretical simulation. **Amir Zada, Asad Ali, Pir Muhammad Ismail**: Formal analysis, Visualization. **Ismail Ahmad, Rahim Shah, Imran Khan, Huahai Shen, Junsong Chen:** Data curation, Investigation. **Chunhua Cui, Xiaoqiang Wu, Qingquan Kong:** Formal analysis. **Jiabao Yi, Xiaotao Zu:** Formal analysis, Data curation. **Fazal Raziq**: Conceptualization, Methodology, Supervision, **Liang Qiao:** Critical review, Supervision, Project administration, Funding acquisition.

Declaration of Competing Interest

The authors declare that they have no known competing financial interests or personal relationships that could have appeared to influence the work reported in this paper.

Acknowledgments

Liang Qiao acknowledges the research support by the National Natural Science Foundation of China (No. 11774044).

Appendix A. Supporting information

Supplementary data associated with this article can be found in the online version at doi:10.1016/j.apcatb.2022.121149.

References

[1] J. Wang, S. Lin, N. Tian, T. Ma, Y. Zhang, H.J.A.F.M. Huang, Nanostructured Metal Sulfides: Classification, Modification Strategy, and Solar-Driven CO_2 Reduction Application, Adv. Funct. Mater. 31 (2021), 2008008.
[2] Z. Huang, K. Teramura, H. Asakura, S. Hosokawa, T.J.C.O.I.C.E. Tanaka, Recent progress in photocatalytic conversion of carbon dioxide over gallium oxide and its nanocomposites, Curr. Opin. Chem. Eng. 20 (2018) 114–121.
[3] Y. Zhao, M. Zhao, X. Ding, Z. Liu, H. Tian, H. Shen, X. Zu, S. Li, L. Qiao, One-step colloid fabrication of nickel phosphides nanoplate/nickel foam hybrid electrode for high-performance asymmetric supercapacitors, Chem. Eng. J. 373 (2019) 1132–1143.
[4] Y. Zhao, C. Huang, Y. He, X. Wu, R. Ge, X. Zu, S. Li, L. Qiao, High-performance asymmetric supercapacitors realized by copper cobalt sulfide crumpled nanoflower and N, F co-doped hierarchical nanoporous carbon polyhedron, J. Power Sources 456 (2020), 228023.
[5] X. Wu, J. He, M. Zhang, Z. Liu, S. Zhang, Y. Zhao, T. Li, F. Zhang, Z. Peng, N. Cheng, J. Zhang, X. Wen, Y. Xie, H. Tian, L. Cao, L. Bi, Y. Du, H. Zhang, L. Qiao, Binary Pd/amorphous-SrRuO3 hybrid film for high stability and fast activity recovery ethanol oxidation electrocatalysis, Nano Energy 67 (2020), 104247.
[6] A. Zada, P. Muhammad, W. Ahmad, Z. Hussain, S. Ali, M. Khan, Q. Khan, M.J.A.F. M. Maqbool, Surface Plasmonic-Assisted Photocatalysis and Optoelectronic Devices with Noble Metal Nanocrystals: Design, Synthesis, and Applications, Adv. Funct. Mater. 30 (2020), 1906744.
[7] A. Zada, M. Humayun, F. Raziq, X. Zhang, Y. Qu, L. Bai, C. Qin, L. Jing, H.J.A.E. M. Fu, Exceptional visible-light-driven cocatalyst-free photocatalytic activity of g-C3N4 by well designed nanocomposites with plasmonic Au and SnO2, Adv. Energy Mater. 6 (2016), 1601190.
[8] T. Ilyas, F. Raziq, S. Ali, A. Zada, N. Ilyas, R. Shaha, Y. Wang, L. Qiao, Design, Facile synthesis of MoS_2/cu as trifunctional catalyst for electrochemical overall water splitting and photocatalytic CO_2 conversion, Mater. Des. 204 (2021), 109674.
[9] F. Raziq, J. He, J. Gan, M. Humayun, M.B. Faheem, A. Iqbal, A. Hayat, S. Fazal, J. Yi, Y. Zhao, K. Dhanabalan, X. Wu, A. Mavlonov, T. Ali, F. Hassan, X. Xang,

X. Zu, H. Shen, L. Qiao, Promoting visible-light photocatalytic activities for carbon nitride based 0D/2D/2D hybrid system: Beyond the conventional 4-electron mechanism, Appl. Catal. B: Environ. 270 (2020), 118870.
[10] A. Mavlonov, T. Razykov, F. Raziq, J. Gan, J. Chantana, Y. Kawano, T. Nishimura, H. Wei, A. Zakutayev, T. Minemoto, X. Zu, S. Li, L. Qiao, A review of Sb_2Se_3 photovoltaic absorber materials and thin-film solar cells, Sol. Energy 201 (2020) 227–246.
[11] Y. Hinuma, T. Kamachi, N. Hamamoto, M. Takao, T. Toyao, K.-I.J.T.J.O.P.C. C. Shimizu, Surface Oxygen Vacancy Formation Energy Calculations in 34 Orientations of β-Ga2O3 and θ-Al2O3, J. Phys. Chem. 124 (2020) 10509–10522.
[12] M. Yang, C. Sun, T. Wang, F. Chen, M. Sun, L. Zhang, Y. Shao, Y. Wu, X.J.A.A.E. M. Hao, Graphene-oxide-assisted synthesis of Ga2O3 nanosheets/reduced graphene oxide nanocomposites anodes for advanced alkali-ion batteries, ACC Appl. Energy Mater. 1 (2018) 4708–4715.
[13] X. Wang, Q. Xu, M. Li, S. Shen, X. Wang, Y. Wang, Z. Feng, J. Shi, H. Han, C.J.A. C. Li, Photocatalytic overall water splitting promoted by an α–β phase junction on Ga2O3, Angew. Chem. Cnternational Ed. 124 (2012) 13266–13269.
[14] H.J. Yoon, J.H. Yang, S.J. Park, C.K. Rhee, Y.J.A.S.S. Sohn, Photocatalytic CO_2 reduction and hydrogen production over Pt/Zn-embedded β-Ga2O3 nanorods, Appl. Surf. Sci. 536 (2021), 147753.
[15] Y. Hou, L. Wu, X. Wang, Z. Ding, Z. Li, X.J.J.O.C. Fu, Photocatalytic performance of α-, β-, and γ-Ga2O3 for the destruction of volatile aromatic pollutants in air, J. Catal. 250 (2007) 12–18.
[16] R. Jangir, S. Porwal, P. Tiwari, P. Mondal, S. Rai, T. Ganguli, S. Oak, S.J.J.O.A. P. Deb, Photoluminescence study of β-Ga2O3 nanostructures annealed in different environments, J. Appl. Phys. 112 (2012), 034307.
[17] J. Xu, W. Zheng, F.J.J.O.M.C.C. Huang, Gallium oxide solar-blind ultraviolet photodetectors: a review, J. Chem. C. 7 (2019) 8753–8770.
[18] M. Wang, G.J.S.R. Lu, Improved Light Harvesting and Efficiency for Overall Water Splitting by Embedding TiO2 Transition Layer in GaP/Ga2O3/Ga2Se3 Multijunction Photocatalyst, Sol. RRL (2021), 2000619.
[19] R. Ito, M. Akatsuka, A. Ozawa, Y. Kato, Y. Kawaguchi, M. Yamamoto, T. Tanabe, T. J.Ao Yoshida, Photocatalytic activity of Ga2O3 supported on Al2O3 for water splitting and CO_2 reduction, ACC OMEGA 4 (2019) 5451–5458.
[20] P.K. Prajapati, A. Kumar, S.L.J.A.S.C. Jain, Engineering, First photocatalytic synthesis of cyclic carbonates from CO_2 and epoxides using CoPc/TiO2 hybrid under mild conditions, ACS Sustain. Chem. Eng. 6 (2018) 7799–7809.
[21] P.-C. Lo, M.S. Rodríguez-Morgade, R.K. Pandey, D.K. Ng, T. Torres, F.J.C.S. R. Dumoulin, The unique features and promises of phthalocyanines as advanced photosensitisers for photodynamic therapy of cancer, Chem. Soc. Rev. 49 (2020) 1041–1056.
[22] Z. Mu, S. Chen, Y. Wang, Z. Zhang, Z. Li, B. Xin, L.J.S.S. Jing, Controlled Construction of Copper Phthalocyanine/α-Fe2O3 Ultrathin S-Scheme Heterojunctions for Efficiently Photocatalytic CO2 Reduction under Wide Visible-Light Irradiation, Small Science, 2100050.
[23] P. Kumar, A. Kumar, B. Sreedhar, B. Sain, S.S. Ray, S.L. Jain, Cobalt phthalocyanine immobilized on graphene oxide: an efficient visible-active catalyst for the photoreduction of carbon dioxide, A Eur. J. -Chem. Eur. (2014).
[24] J.P. Perdew, A. Ruzsinszky, G.I. Csonka, O.A. Vydrov, G.E. Scuseria, L. A. Constantin, X. Zhou, K. Burke, Restoring the Density-Gradient Expansion for Exchange in Solids and Surfaces, Phys. Rev. Lett. 100 (2008), 136406.
[25] G. Kresse, J. Furthmüller, Efficiency of ab-initio total energy calculations for metals and semiconductors using a plane-wave basis set, Comput. Mater. Sci. 6 (1996) 15–50.
[26] G. Kresse, J. Furthmüller, Efficient iterative schemes for total-energy calculations using a plane-wave basis set, Phys. Rev. B 54 (1996) 11169–11186.
[27] G. Kresse, J. Hafner, Ab initio molecular dynamics for liquid metals, Phys. Rev. B 47 (1993) 558–561.
[28] S. Grimme, J. Antony, S. Ehrlich, H. Krieg, A consistent and accurate ab initio parametrization of density functional dispersion correction (DFT-D) for the 94 elements H-Pu, J. Chem. Phys. 132 (2010), 154104.
[29] R. Bader, Atoms in Molecules: A Quantum Theory Oxford University Press, (1990).
[30] G. Henkelman, A. Arnaldsson, H. Jónsson, A fast and robust algorithm for Bader decomposition of charge density, Comput. Mater. Sci. 36 (2006) 354–360.
[31] J.K. Nørskov, J. Rossmeisl, A. Logadottir, L. Lindqvist, J.R. Kitchin, T. Bligaard, H. Jónsson, Origin of the Overpotential for Oxygen Reduction at a Fuel-Cell Cathode, J. Phys. Chem. B 108 (2004) 17886–17892.
[32] T. Shao, P. Zhang, L. Jin, Z.J.A.C.B.E. Li, Photocatalytic decomposition of perfluorooctanoic acid in pure water and sewage water by nanostructured gallium oxide, Appl. Catal. B: Environ. 142 (2013) 654–661.
[33] B. Khan, F. Raziq, M.B. Faheem, M.U. Farooq, S. Hussain, F. Ali, A. Ullah, A. Mavlonov, Y. Zhao, Z. Liu, H. Tain, H. Shen, X. Zu, S. Li, H. Xiao, X. Xiang, L. Qiao, Electronic and nanostructure engineering of bifunctional MoS_2 towards exceptional visible-light photocatalytic CO_2 reduction and pollutant degradation, J. Hazard. Mater. 381 (2020), 120972.
[34] F. Raziq, M. Humayun, A. Ali, T. Wang, A. Khan, Q. Fu, W. Luo, H. Zeng, Z. Zheng, B. Khan, H. Shen, X. Zu, S. Li, L. Qiao, Synthesis of S-Doped porous g-C_3N_4 by using ionic liquids and subsequently coupled with Au-TiO_2 for exceptional cocatalyst-free visible-light catalytic activities, Appl. Catal. B: Environ. 237 (2018) 1082–1090.
[35] H.J. Bae, T.H. Yoo, Y. Yoon, I.G. Lee, J.P. Kim, B.J. Cho, W.S.J.N. Hwang, High-Aspect Ratio β-Ga2O3 Nanorods via Hydrothermal Synthesis, nanomaterials 8 (2018) 594.
[36] X. Tan, G. Chen, D. Xing, W. Ding, H. Liu, T. Li, Y.J.E.S.N. Huang, Indium-modified Ga 2 O 3 hierarchical nanosheets as efficient photocatalysts for the degradation of perfluorooctanoic acid, Environ. Sci. Nano 7 (2020) 2229–2239.
[37] M. Domínguez, E. Taboada, H. Idriss, E. Molins, J.J.J.O.M.C. Llorca, Fast and efficient hydrogen generation catalyzed by cobalt talc nanolayers dispersed in silica aerogel, J. Mater. Chem. 20 (2010) 4875–4883.
[38] F. Raziq, L. Sun, Y. Wang, X. Zhang, M. Humayun, S. Ali, L. Bai, Y. Qu, H. Yu, L.J.A. E.M. Jing, Synthesis of large surface-area g-C3N4 comodified with MnOx and Au-TiO2 as efficient visible-light photocatalysts for fuel production, Adv. Energy Mater. 8 (2018), 1701580.
[39] K.A. Mengle, G. Shi, D. Bayerl, E. Kioupakis, First-principles calculations of the near-edge optical properties of β-Ga2O3, Appl. Phys. Lett. 109 (2016), 212104.
[40] H. Yuan, J. Su, R. Guo, K. Tian, Z. Lin, J. Zhang, J. Chang, Y. Hao, Contact barriers modulation of graphene/β-Ga2O3 interface for high-performance Ga2O3 devices, Appl. Surf. Sci. 527 (2020), 146740.
[41] M. Chu, K. Hu, J. Wang, Y. Liu, S. Ali, C. Qin, L.J.A.C.B.E. Jing, Synthesis of g-C3N4-based photocatalysts with recyclable feature for efficient 2, 4-dichlorophenol degradation and mechanisms, Appl. Catal. B: Environ. 243 (2019) 57–65.
[42] F. Raziq, A. Hayat, M. Humayun, S.K.B. Mane, M.B. Faheem, A. Ali, Y. Zhao, S. Han, C. Cai, W. Li, D.C. Qi, X. Yu, M.B.H. Breese, F. Hassan, A. Mavlonov, K. Dhanabalan, L. Qiao, Photocatalytic solar fuel production and environmental remediation through experimental and DFT based research on CdSe-QDs-coupled P-doped-g-C_3N_4 composites, Appl. Catal. B: Environ. 270 (2020), 118867.
[43] A. Zada, Y. Qu, S. Ali, N. Sun, H. Lu, R. Yan, X. Zhang, L.J.J.O.H.M. Jing, Improved visible-light activities for degrading pollutants on TiO2/g-C3N4 nanocomposites by decorating SPR Au nanoparticles and 2, 4-dichlorophenol decomposition path, J. Hazard. Mater. 342 (2018) 715–723.
[44] H. Li, Z. Zhao, Q. Cai, L. Yin, J. Zhao, Nitrogen electroreduction performance of transition metal dimers embedded into N-doped graphene: a theoretical prediction, J. Mater. Chem. A 8 (2020) 4533–4543.